JCTC Journal of Chemical Theory and Computation

Article

pubs.acs.org/JCTC

Can Multiconfigurational Self-Consistent Field Theory and Density Functional Theory Correctly Predict the Ground State of Metal–Metal-Bonded Complexes?

Rebecca K. Carlson, Samuel O. Odoh, Stephen J. Tereniak, Connie C. Lu, and Laura Gagliardi*

Department of Chemistry, Chemical Theory Center, and Supercomputing Institute, University of Minnesota, Minneapolis, Minnesota 55455, United States

Supporting Information

ABSTRACT: The electronic structure of a diiron (FeFe) complex with strong metal–metal interaction and those of analogous complexes (CoCo, CoMn, CoFe, and FeMn) with much weaker metal–metal bonding are investigated with wave function-based methods and density functional theory. The delocalization and bonding between the metal centers in the diiron complex is only fully captured after inclusion of the complete set of 3*d* and 4*d* orbitals in the active space, a situation best suited for restricted active space (RAS) approaches. Truncation of the included set of 4*d* orbitals results in inappropriate localization of some 3*d* orbitals, incorrect description of the ground spin state as well as wrong spin state energetics, as compared to experiment. Using density functional theory, some local functionals are able to predict the correct ground spin states, and describe the chemical bonding and structural properties of all the metal–metal complexes considered in this work. In contrast, the introduction of some exact exchange results in increased localization of 3*d* orbitals and wrong spin state energetics, a situation that is particularly troublesome for the diiron complex.

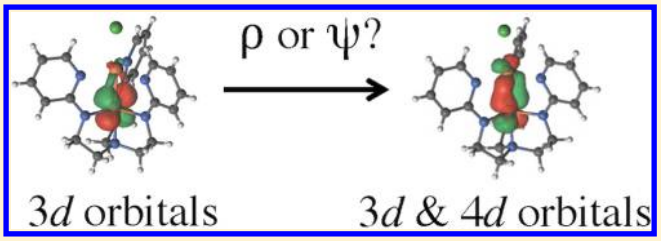

INTRODUCTION

One of the outstanding challenges for quantum mechanical methods relates to the accurate treatment of multireference systems to fully account for electron correlation effects. In general, multireference systems are those that cannot be qualitatively correctly described by a single electronic configuration. Electronic correlation energy, according to Löwdin, is defined as the difference between the exact energy of a Hamiltonian and the Hartree–Fock (HF) energy using the same Hamiltonian.[1] The special types of errors that occur in a single-reference formalism, where one Slater determinant (SD) or configuration state function (CSF) is used, are called "static" or "non-dynamical" correlation errors.[2−4] Particularly, systems containing transition metals are often multiconfigurational and in order to accurately describe their structural properties, electronic structure and catalytic properties, a proper treatment of static electron correlation is needed.

Kohn–Sham density functional theory (KS-DFT)[5] is a very popular method. It has been applied to a large number and variety of systems and is particularly amenable for studying large molecules that are often intractable with wave function based methods.. However, as KS-DFT is a single determinantal method, the accuracy achievable with existing functionals is typically low for inherently multiconfigurational systems.[6−8] In addition, there have been many cases in which various exchange-correlation functionals give conflicting results for multiconfigurational systems. This problem often occurs in the prediction of the ground spin states of transition metal complexes. In general, hybrid functionals favor high-spin states, while generalized gradient approximation (GGA) functionals favor low-spin states.[9,10] Truhlar et al.,[11] Swart,[12] and Reiher et al.[13] have shown that the relative spin state energies of various iron-containing systems depend on the type of functional and the amount of exact HF exchange used. Another complication that arises in KS-DFT is the existence of broken symmetry[14,15] solutions. While breaking symmetry constraints allows for a variationally lower energy solution that may be more accurate in energy,[11] ambiguous spin states may result from optimizing a wave function for a nonphysical state.

As an alternative to KS-DFT, multiconfiguration self-consistent-field (MCSCF) approaches, such as the complete active space self-consistent field (CASSCF)[16] method, are used to study the properties of inherently multiconfigurational systems. These methods can account for static electron correlation effects. Dynamic correlation effects can then be added by multireference perturbation theory [such as complete-active-space second-order perturbation theory (CASPT2)[17]] or multireference configuration interaction (MRCI)[18] methods, using the MCSCF wave function as a reference, to achieve quantitative accuracy. Such methods are generally considered as the standards to which to compare results obtained with different exchange-correlation density functionals.[19,20]

Received: May 4, 2015
Published: July 27, 2015

ACS Publications © 2015 American Chemical Society

DOI: 10.1021/acs.jctc.5b00412
J. Chem. Theory Comput. 2015, 11, 4093−4101

CASSCF/CASPT2 is a popular multireference method. However, in CASSCF the major drawback is that the number CSFs or SDs scales exponentially with the number of active orbitals. CASSCF/CASPT2 calculations with more than 18 electrons in 18 active orbitals are not currently feasible, and this limits the type of chemical problems that can be addressed with such a method. One can employ larger active spaces and still reduce the computational cost associated with CASSCF/CASPT2 by imposing constraints on the active space using the restricted active space (RASSCF)[21] and generalized active space (GASSCF)[22] self-consistent field methods. Other wave function methods aimed at reducing the size of the CI expansion include SplitGAS,[23] occupation-restricted-multiple-active-space (ORMAS) SCF methods,[24,25] and DMRG.[26−30] We have also recently developed a method, multiconfiguration pair-density functional theory (MC-PDFT),[31] that incorporates multiconfigurational character into the density, avoiding the need for the broken-symmetry solutions that exist in KS-DFT.

Most studies on metallic systems with multiconfigurational character have focused on monometallic complexes,[12,32] particularly heme complexes[20,33] with much fewer studies performed on bimetallic, multiply bonded metal−metal complexes. In the present work, we are interested in examining the electronic structure of bimetallic complexes that contain first-row transition metals in a trigonal ligand scaffold, as synthesized by Lu and co-workers, Figure 1.[34,35] In particular,

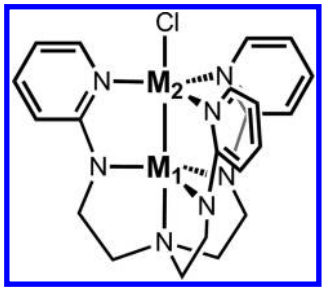

Figure 1. Structure of the M_1-M_2-Cl series of complexes. These complexes possess a *N,N,N*-tri(2-(2-pyridylamino)ethyl)amine ligand scaffold and two 1st row transition metals that are labeled as M_1 (bottom metal) and M_2 (top metal). There are three nitrogen atoms in the equatorial regions of the metal atoms, while M_1 also has a apical nitrogen.

we are interested in the electronic structure properties of the diiron chloride analogue of the M_1-M_2-Cl series with the pyridine scaffold, where M_1 and M_2 represent the identity of a transition metal in Figure 1.[34] The interest in this particular complex arises from the fact that, while the electronic structures of the various $Co-M_2-Cl$ (Co−Co−Cl, Co−Mn−Cl, and Co−Fe−Cl) and Fe−Mn−Cl species were well described by various theoretical methods, it was found that attaining the correct electronic structure properties for the Fe−Fe−Cl analogue was more challenging. The Fe−Fe−Cl complex is all the more interesting as it was empirically found to be an outlier from the available series of M_1-M_2-Cl complexes as it possesses a septet spin ground state with ferromagnetic coupling of the two iron centers, in stark contrast to all other complexes in this series which were found to possess low spin ground states formed by antiferromagnetically coupling two high spin metal sites.[34] In this article, we present an in-depth theoretical study of the Fe−Fe−Cl complex and explain the differences between this particular complex and other members of the M_1-M_2-Cl series.

COMPUTATIONAL METHODS

Wave Function Calculations. All the CASSCF/CASPT2 and RASSCF/RASPT2[36] (RASPT2 is a second-order perturbation on a RASSCF wave function) calculations were performed using the MOLCAS 7.8 package[37] on the experimental X-ray structures. The active space choices, denoted (n, m) for the CASSCF calculations, included all 3*d* electrons n of the transition metals in m 3*d* and 4*d* orbitals. For Fe−Fe−Cl, the CASSCF active spaces used were (12,12), (12,14), and (12,15) which include all the 3*d* electrons and orbitals and an additional two, four, or five 4*d* orbitals, respectively. The active space choice for the RASSCF calculations is denoted by (12,20)/(12,10)/2. The first set of parentheses corresponds to the total number of electrons in RAS1 and RAS2 and the total number of orbitals in all of the RAS spaces. The second set of parentheses corresponds to the number of active electrons and orbitals in RAS2; the final value of 2 indicates the number of particles allowed into RAS3. In addition, we also performed RAS-CI calculations with the (12,20)/(12,10)/2 active space for the Fe−Fe−Cl complex, optimizing the CI expansion for each spin state without optimizing the orbitals for each spin state. For these RAS-CI calculations, the orbitals were obtained from the septet RASSCF (12,20)/(12,10)/2 calculation and used for all spin states and we only reoptimized the CI coefficients for each state.

All calculations utilized the Douglas-Kroll-Hess Hamiltonian[38] to account for relativistic effects and used the relativistic all-electron ANO-RCC basis sets on all atoms in the complexes. Specifically, double-ζ quality (ANO-RCC-VDZP)[39,40] basis sets were used for Co, Fe, N, and Cl atoms and minimal basis sets (ANO-RCC-MB)[40] were used for C and H atoms. The following contractions were employed: [5s4p2d1f] for all the metal atoms, [3s2p1d] for the nitrogen and chlorine, [2s1p] for the carbon atoms, and [1s] for the hydrogen atoms. Reduction of the four center 2-electron integrals to effective three center integrals via auxiliary basis sets was accomplished with the RICD approximation.[41] For the CASPT2/RASPT2 calculations, an imaginary level shift of 0.2 a.u. (atomic units) was used to prevent the occurrence of intruder states.[42] The effective bond orders (EBO)[43] between the atoms in these complexes were calculated at the electronic ground state. The EBO is defined as the difference of the sum of the bonding orbital occupations and the sum of the antibonding orbital occupation numbers divided by two.

DFT Calculations. All the DFT calculations were performed using the ADF 2013 package.[44] The scalar-relativistic zeroth order regular approximation (ZORA) was employed to include relativistic effects.[45,46] In all DFT calculations, all-electron Slater type orbitals of triple-ζ quality with two polarization functions (TZ2P) were used to describe all atoms. Three classes of functionals were used to calculate the relative energies of the various spin states of the M_1-M_2-Cl complexes at the structures obtained from X-ray crystallography experiments.[34] The first are local functionals, namely, LDA,[47] BLYP,[48,49] PBE,[50,51] TPSS,[52] and the Minnesota M06-L[53,54] functional. The effect of exact exchange was investigated by considering the PBE0-12%, PBE0-25%, and PBE0-50% functionals. For these hybrid functionals, the notation -x% denotes the fraction of Hartree−Fock exchange

DOI: 10.1021/acs.jctc.5b00412
J. Chem. Theory Comput. 2015, 11, 4093−4101

included in a PBE0-type functional. As an example, PBE0-12% contains 12% exact exchange, instead of 25% as used in the original PBE0 (here labeled as PBE0-25%) functional.[50] Calculations were also carried out with the B3LYP[49,55,56] functional, to allow for comparison with BLYP. The last class of functionals contains the TPSSh[52] functional as well as two of the Minnesota 06 metahybrid functionals, M06 and M06-2X.[53,54] All these calculations were carried out within the unrestricted DFT formalism.

To examine the performance of the various density functionals for predicting the structures of the metal−metal complexes, geometry optimizations were carried out in the gas phase without symmetry constraints. In these geometry optimizations, we have used only the LDA, PBE, PBE0-12%, PBE0, and M06 functionals. The geometry optimizations were followed by vibrational frequency analyses to confirm that the optimized structures were local minima. More details about the calculations are presented in the Supporting Information section.

RESULTS AND DISCUSSION

Multiconfigurational Calculations. All the metals in the bimetallic complexes considered in this work are formally in the +2 oxidation state. A minimal active space includes the 3*d* electrons from each of the metals in an orbital space of all ten 3*d* orbitals. On the basis of previous experience with similar complexes, we found that including some, but not all, of the correlating 4*d* shell is enough to accurately describe the wave function of these M_1-M_2-Cl complexes.[34,35,57]

A suitable active space for the three $Co-M_2-Cl$ and Fe−Mn−Cl complexes in our calculations included all the 3*d* electrons in all the 3*d* orbitals, as well as two additional 4*d* correlating orbitals, for a total of 12 orbitals. However, this active space was found to be insufficient for capturing the septet state as the correct ground state, based on experimental studies, of the Fe−Fe−Cl complex. We explored larger active spaces to see if we could accurately predict the correct ground state and capture the electronic structure properties of Fe−Fe−Cl. The following active spaces were attempted for all spin states: (12,12), (12,14), (12,15). For the singlet and triplet spin states, CASSCF calculations with the (12,15) active space were not feasible due to the large number of configurations state functions (Table S1) and the slow convergence of the CI expansion with concomitant orbital relaxation. However, to qualitatively describe all the spin states of Fe−Fe−Cl while using larger active spaces, we carried out RAS-CI calculations for the different spin states while using the orbitals obtained from the septet electronic state of the (12,20)/(12,10)/2 calculation and only reoptimized the CI coefficients for each state. For the (12,12), (12,14), and (12,20)/(12,10)/2 active spaces, the relative spin state energies of Fe−Fe−Cl are presented in Table 1.

There are several important things to note. First, the singlet state is always predicted to be the lowest in energy for the Fe−Fe−Cl complex at the CASSCF and RASCI levels. Second, as the π/π^* pairs of orbitals are not present when the active space contains less than 20 orbitals, the inclusion of the full 20 orbitals has a significant effect on the calculated relative energies, as well as on the bonding between the two iron centers. To illustrate, the EBO between the metal centers, as well as the weights of the d_{xz} and d_{yz} orbitals in the π molecular orbital are shown in Table 2 for the septet wave function for different active space sizes. For the (12,12) and (12,14) active spaces, the d_{xz} and d_{yz} orbitals in the π molecular orbital are largely localized, with little mixing or delocalization, and have an EBO of about 0.2. Only once the active space is sufficiently increased to (12,20)/(12,10)/2 does a delocalized bonding scheme (25.6% and 74.4% weight of the d_{xz} and d_{yz} orbitals in the π molecular orbital between the two metals) between the metals appear, consistent with a much larger EBO of 0.73.

Table 1. Relative Spin State Energies (kcal/mol) of the Fe−Fe−Cl Complex for Various Active Spaces with Respect to the Energy of the Septet State

	(12,12)		(12,14)		(12,20)/(12,10)/2	
	CASSCF	CASPT2	CASSCF	CASPT2	RASCI	RASPT2
singlet	−5.1	−8.7	−6.3	−3.1	−1.6	1.5
triplet	−4.7	−4.3	−5.5	−1.2	−1.3	1.6
quintet	−2.7	−4.4	−3.9	0.6	−1.2	−0.1
septet	0.0	0.0	0.0	0.0	0.0	0.0
nonet	11.8	0.7	−1.1	−5.3	3.9	2.0

Table 2. EBO, Weight of Dominant Configuration (DC), and Percent Distribution of d_{xz} and d_{yz} Components between the Fe Centers of the π Symmetry Molecular Orbitals for the Septet Spin State of Fe−Fe−Cl

active space	EBO	weight of DC (%)	% of d_{xz} and d_{yz} in the π symmetry MO
(12,12)	0.18	27.3	Completely localized
(12,14)	0.22	28.6	1.5% and 98.5%
(12,20)/(12,10)/2	0.73	28.0	25.6% and 74.4%

Second, the expansion of the active space size alters the relative energies of the various spin states. For the calculations employing 12 electrons in 12 active orbitals, the nonet state is about 17 kcal/mol higher in energy than the singlet state with CASSCF. Such calculations include only σ/σ^* pairs. As the active space is enlarged to include more 4*d* orbitals of the metals, the bonding orbital becomes more delocalized and the nonet state becomes lower in energy. Once the active space is increased to include all ten 3*d* in RAS2 and all ten 4*d* in RAS3, it results in spin states that are much closer in energy at the SCF level, Table 1.

Third, with perturbation methods, it appears that there is a large effect from dynamic correlation, Table 1. For the (12,12) active space, the singlet is still predicted to be the ground state, although the nonet is lowered in energy and is predicted to be only about 1 kcal/mol higher than the septet. Expansion of the active space to (12,14), results in a nonet ground state with the quintet and triplet states also slightly higher in energy than the septet. Neither the CASSCF nor CASPT2 are converged with respect to these smaller active space sizes. However, the relative energies of the spin states obtained at the RASPT2 level are all within 2 kcal/mol. It should be noted that since in the RASSCF (12,20)/(12,10)/2 calculations the orbitals were optimized only for the septet case, while for the other spin states only the CI coefficients were optimized (see Computational Methods), the spin state energy spacings are probably larger than if the orbitals had been optimized for each state. Table 3 show the septet-nonet splitting as a function of the active space size and confirms that in the (12,20)/(12,10)/2 case the energy splitting is reduced using the MCSCF orbitals for each spin state, rather than the septet orbitals for both states.

A full RASSCF calculation with 20 orbitals was feasible only for the septet and nonet states. As shown in Table 3, as more

DOI: 10.1021/acs.jctc.5b00412
J. Chem. Theory Comput. 2015, 11, 4093−4101

Table 3. Relative Spin State Energies (kcal/mol) of the Septet and Nonet Spin States of Fe−Fe−Cl Obtained at the CASPT2 and RASPT2 Levels of Theory

	(12,12)[a]	(12,14)[a]	(12,15)[a]	(12,20)/(12,10)/2[b]	(12,20)/(12,10)/2[c]
septet	0.0	0.0	0.0	0.0	0.0
nonet	0.7	−5.3	−3.7	−0.02	2.0

[a](12,12), (12,14), (12,15) active spaces for CASSCF/CASPT2 calculations using MCSCF orbitals for each spin state. [b](12,20)/(12,10)/2 active space for a RASSCF/RASPT2 calculation using MCSCF orbitals for each spin state. [c](12,20)/(12,10)/2 active space for a RASCI/RASPT2 calculation using orbitals obtained for the septet state.

Table 4. Occupation of the Active Molecular Orbitalis in the Dominant Configurations in the Fe−Fe−Cl (12,20)/(12,10)/2 Wave Function

config.	σ	σ^*	π	π^*	δ	δ^*	W[a] (%)	S[b]
A	2	0	4	2	2	2	28	3/2
B	0	2	4	2	2	2	5	3/2
C	2	0	2	4	2	2	6	3/2
D	0	2	2	4	2	2	3	3/2
total							42	
E (×2)	1	1	4	2	3	1	14	1 and 2
F (×2)	1	1	4	2	1	3	12	1 and 2
G (×2)	1	1	2	4	3	1	5	1 and 2
H (×2)	1	1	2	4	1	3	5	1 and 2
total							36	

[a]W is the weight of the configuration in the (12,20)/(12,10)/2 calculation. For the configurations with ×2 (two configurations), the weight is sum of the two configurations. [b]S is the spin on the metal center. In A−D, both metals are S = 3/2, and in E−H, one is S = 1 and the other S = 2.

4*d* orbitals are added up to the full 4*d* shell, the splitting between the septet and nonet states decreases until these are nearly degenerate. While the (12,12) active space was sufficient[34] for Co−Co−Cl, Co−Fe−Cl, Co−Mn−Cl, and Fe−Mn−Cl it is evident from Table 2 that the active space is not converged as the total energy splitting for the Fe−Fe−Cl complex decreases dramatically from (12,12) to (12,20), with the relative energies between the septet and nonet states fluctuating.

The dominant configuration of the CASSCF (12,14) and (12,15) septet states is $(\sigma)^2(\mathrm{Fe}_1\ d_{xz})^2(\mathrm{Fe}_1\ d_{yz})^1(\mathrm{Fe}_2\ d_{xz})^1(\mathrm{Fe}_2\ d_{yz})^2\ (\delta)^2(\delta^*)^2(\sigma^*)^0$, similar to what was obtained for Co−Co−Cl. In contrast, for the RASSCF (12,20)/(12,10)/2 active space, the wave function is $(\sigma)^2(\pi)^4(\pi^*)^2(\delta)^2(\delta^*)^2(\sigma^*)^0$ and is delocalized. The weights of the dominant configurations, DC are listed in Table 2. The EBO obtained from the RASSCF (12,20)/(12,10)/2 calculation is much higher than those obtained from the CASSCF calculations and also stands in contrast to those obtained for the other complexes in the series (Co_1−M−Cl = 0.22, Fe−Mn−Cl = 0.31).[34] All these results illustrate that for Fe−Fe−Cl, active spaces with a full 4*d* shell are necessary to capture the stronger metal−metal interactions and electron delocalization across the metal−metal distance.

Even though both the Co−Co−Cl and Fe−Fe−Cl are multiconfigurational, the Co−Co−Cl is well described by two localized S = 3/2 metal centers that are antiferromagnetically coupled to form an overall spin singlet and all levels of theory predict a singlet ground state (vida infra). In contrast, Fe−Fe−Cl has a more complicated multiconfigurational wave function. In Table 4, we report the dominant configurations in Fe−Fe−Cl, which we call A−H. Configurations A−D account for about 42% of the total (12,20)/(12,10)/2 wave function and can be described by two ferromagnetically coupled S = 3/2 metal centers. In A and B, the π^*, δ, and δ^* are singly occupied, while in C and D, the π, δ, and δ^* are singly occupied.

On the other hand, configurations E−H can individually be described by a S = 2 and a S = 1 metal center. For E and F (G and H), the $\pi^*(\pi)$ orbitals are singly occupied, and compared to A−D, one of the four δ/δ^* orbitals is doubly occupied, leaving two singly occupied and one unoccupied. These configurations account for about 36% of the (12,20)/(12,10)/2 wave function. However, configurations E−H, on average, would lead to two S = 3/2 metal centers. The interplay of these two groups of configurations certainly leads to a complicated electronic structure that is not well described by all levels of theory.

The Mulliken 3*d* and 4*d* spin densities for the (12,15) and (12,20)/(12,10)/2 active spaces are shown in Figure 2. Overall, the spin densities of the 3*d* orbitals obtained from the calculation employing the (12,15) active space are unevenly distributed between the two metals within each 3*d* AO type. As an example, the $3d^0$ spin densities are 0.70 for Fe_1 and 0.35 for Fe_2. In contrast, the 3*d* spin density distribution is more evenly distributed between the two Fe centers for the (12,20)/(12,10)/2 active space. For example, the $3d^0$ orbital spin density is 0.55 and 0.49 for Fe_1 (bottom Fe) and Fe_2 (top Fe), respectively, Figure 2a. This more even distribution of spin density reflects the increased delocalized nature of the *d*-orbital electron density that is expected for a shorter M−M distance compared to the other M_1−M_2−Cl complexes in the series. The difference in the total Mulliken spin density of all atomic basis functions for each metal is smaller once a full 4*d* shell is added, suggesting a more even distribution of the density. For the (12,15) active space, Fe_1 has a total spin density of 2.8740 and Fe_2 has a spin density of 2.9596, a difference of 0.0856 between the two metals. For the (12,20)/(12,10)/2 active space, the difference decreases to 0.0581, with a spin density of 2.8858 and 2.9439 on Fe_1 and Fe_2, respectively.

For the 4*d* orbitals, the spin density on Fe_1 for both active spaces is relatively unchanged, but increases slightly for Fe_2 with a full 4*d* shell. For $4d^{2+}$ on Fe_2, the spin density increases from 0.0047 to 0.0076 with the (12,20)/(12,10)/2 active space. This occurs despite the fact that the addition of the full 4*d* set of orbitals is primarily responsible for the more even distribution of spin density (greater delocalized picture) between the metals, as well as the nearly degenerate spin state spectrum, Table 1. In Figure 2a, the spin density shifts between the two metals for the (12,15) active space and becomes more evenly distributed for the (12,20)/(12,10)/2 active space. In Figure 2b, the spin density for the correlating shell is shown. For the (12,15) active space, most of the spin density is on the bottom metal. Once the full 4*d* shell is added, the red curve in Figure 2b shifts up to the purple curve.

To conclude this section about the active space dependence in the Fe−Fe−Cl case, we discuss one last item. The final result of a CASSCF or RASSCF calculation may depend on the starting orbitals. We then decided to repeat the calculations with the smaller active spaces, (12,12), (12,14) and (12,15), starting from the RASSCF orbitals of the (12,20)/(12,10)/2 calculation. The purpose of this test was to check if by starting from delocalized orbitals (those from the (12,20)/(12,10)/2

DOI: 10.1021/acs.jctc.5b00412
J. Chem. Theory Comput. 2015, 11, 4093−4101

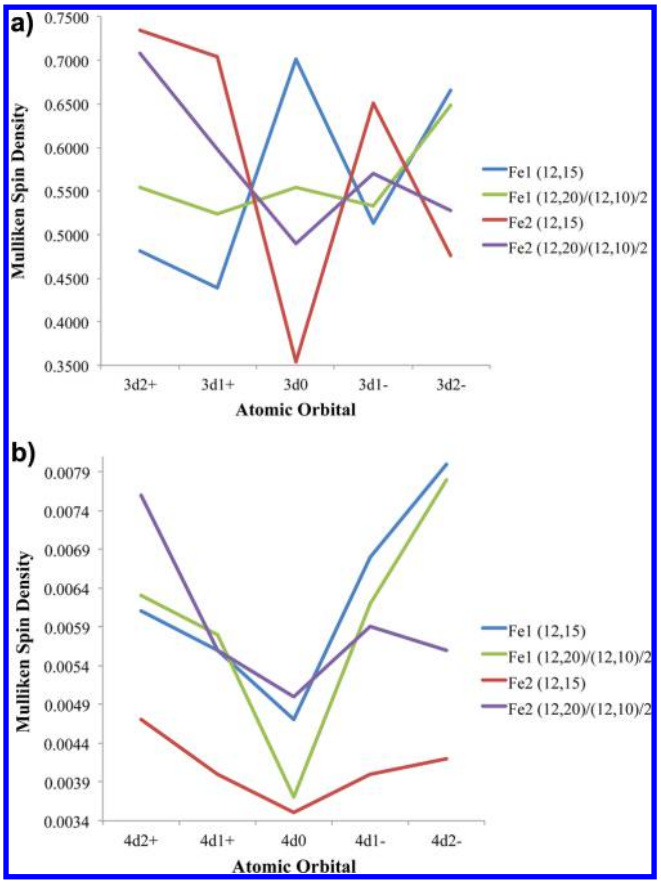

Figure 2. (a) Mulliken spin density plot of 3*d* orbitals for Fe−Fe−Cl for the (12,15) and (12,20)/(12,10)/2 active spaces. (b) Mulliken spin density plot of 4*d* orbitals for Fe−Fe−Cl for the (12,15) and (12,20)/(12,10)/2 active spaces.

calculation), one could still maintain delocalization, even when reducing the active space. Instead, in all cases we converged to the same states as previously obtained with the smaller CASSCF spaces, that is, the energy was the same, and the MOs were localized again.

In Figure 3, we show that the (12,20)/(12,10)/2 active space contains a 4*d* orbital of σ-character, two of π/ π*-character, and two δ/ δ*-type orbitals, while there are no π bonding orbitals for the (12,15) active space.

Isostructural Co−Co−Cl Complex. It is important to determine why the inclusion of the full 4*d*-shell results in the alteration of the relative energies of the various spin states of Fe−Fe−Cl complex, Tables 1 and 3. Insights into the effect of the *4d*-shell can be obtained by comparing Fe−Fe−Cl to other members of the M_1−M_2−Cl series. To this end, similar calculations were performed for the analogous Co−Co−Cl complex using fully optimized orbitals for each spin state. The relative energies between the singlet, triplet, quintet and septet states of Co−Co−Cl obtained with the (14,12) and (14,20)/(14,10)/2 active spaces are presented in Table 5. To summarize, the singlet state remains the ground state of Co−Co−Cl, which is consistent with experiment, regardless of active space size. Additionally, the relative energies of the higher spin states obtained with the (14,12) active space are generally within 2 kcal/mol of those obtained with the (14,20)/(14,10)/2 active space, suggesting that additional 4d orbitals play little role in the ordering of these spin states of Co−Co−Cl.

As we did for Fe−Fe−Cl, we now examine the electronic configuration of Co−Co−Cl. It was found that the dominant configuration obtained from calculations with (14,12), (14,14), and (14,20)/(14,10)/2 active spaces for the singlet ground state of Co−Co−Cl is $(\sigma)^2(Co_2\ 3d_{yz})^2(Co_2\ 3d_{xz})^2(Co_1\ 3d_{yz})^2(Co_1\ 3d_{xz})^2(Co_1\ 3d_{xy})^1(Co_1\ 3d_{x^2-y^2})^1(Co_2\ 3d_{xy})^1(Co_2\ 3d_{x^2-y^2})^1\ (\sigma^*)^0$. A qualitative MO diagram for Co−Co−Cl can be found in Figure S3. The weight of this configuration and the EBO obtained for the different active space sizes are shown in Table 6. Although, the weight of the dominant configuration decreases slightly after addition of a full 4*d* shell to the active space, the EBO and the average occupation numbers are relatively unchanged. Overall, these results suggest that the 4*d* shell has a minimal impact on the electronic structure and bonding in Co−Co−Cl, in stark contrast to the situation obtained for Fe−Fe−Cl.

Density Functional Theory Approaches. Given the significant multiconfigurational character of the wave functions of the M_1−M_2−Cl complexes, it is reasonable to expect that the suitability of DFT for studying their electronic, structural and chemical reaction properties will be limited. DFT however offers significant computational savings over correlated wave function approaches. For this reason, it is important to determine the performance of various exchange-correlation functionals for capturing the properties of these complexes.

Relative Energies of Various Spin States. The relative energies of the various spin states of the Fe−Fe−Cl complex were calculated with the LDA, PBE, BLYP, TPSS, M06-L, B3LYP, TPSSh PBE0-12%, PBE0-25%, PBE0-50%, M06, and M06-2X functionals, at the X-ray crystal structure. LDA predicts Fe−Fe−Cl to have a septet ground state while PBE and BLYP predict the septet and triplet spin states of Fe−Fe−Cl as being degenerate, Figure 4. In contrast, although the meta-GGA functionals TPSS and M06-L both also predict the septet and triplet states to be close in energy, Figure 4, M06-L in particular appears to favor the high spin Fe(II) nonet and broken-symmetry singlet states by 6.0 and 4.3 kcal/mol relative to the septet state, respectively.

Since LDA, BLYP, and PBE predict the correct ground state for Fe−Fe−Cl, we tested them also for the other M_1−M_2−Cl complexes and calculated the relative energies of the various spin states of the Co−Co−Cl, Co−Fe−Cl, Co−Mn−Cl, and Fe−Mn−Cl complexes. All the three functionals LDA, BLYP, and PBE predict doublet ground states for Co−Fe−Cl and Fe−Mn−Cl, the broken-symmetry singlet state for Co−Co−Cl and the triplet state for Co−Mn−Cl complex (see Supporting Information for details), in agreement with experimental assignments.

For Fe−Fe−Cl, addition of exact exchange to the PBE functional leads to the stabilization of the nonet and singlet states relative to the septet state, Figure 4. To illustrate, with the local PBE functional, the nonet state is about 15 kcal/mol less stable than the septet state. Addition of 12% exact exchange reduces this energy difference to about 3 kcal/mol. As noted previously, the nonet and singlet states have high spin Fe(II) ions. As the amount of exact exchange is increased from 12% in PBE0-12% to 50% in PBE0-50%, these high-spin Fe(II) states become more stable than the septet state. A similar stabilization of the nonet state is obtained when the hybrid B3LYP, as well as the meta-hybrid TPSSH, M06, and M06-2X functionals are used, Figure 4. The propensity of hybrid functionals toward stabilization of the high-spin states of metal complexes is expected from literature experience.[13,58,59] However, our

DOI: 10.1021/acs.jctc.5b00412
J. Chem. Theory Comput. 2015, 11, 4093−4101

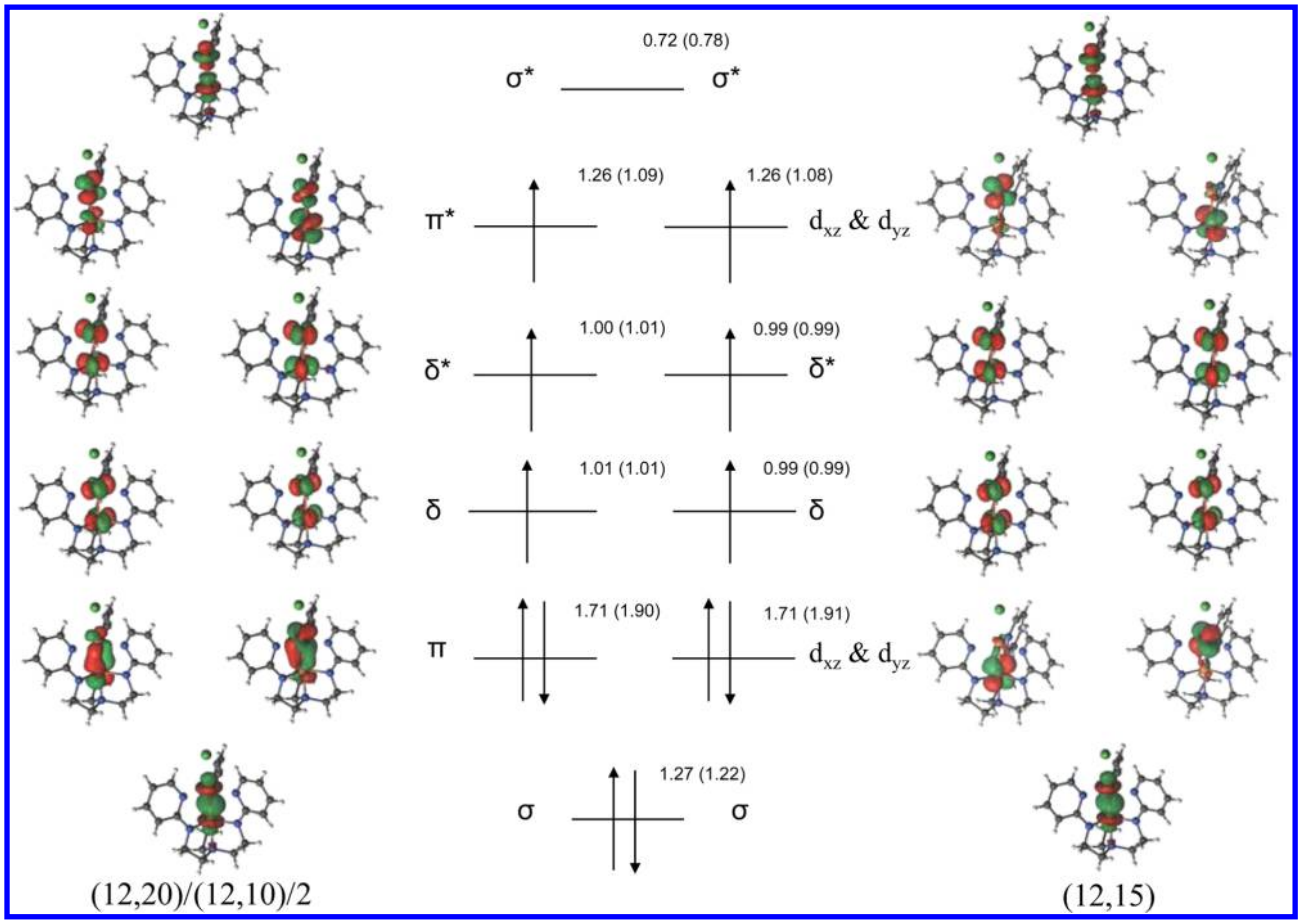

Figure 3. Qualitative orbital diagrams for the 3*d* orbitals computed with the (12,20)/(12,10)/2 and (12,15) active spaces. The natural orbital occupation numbers obtained for these orbitals in the (12,20)/(12,10)/2 calculation are shown while those corresponding to the (12,15) active space are given in parentheses. Note that the (12,15) MO diagram shows a more localized bonding manifold, similar to the other M−M−Cl complexes, especially for the π and π^* orbitals. This is in contrast to the larger (12,20)/(12,10)/2 active space which shows significant delocalization in these particular orbitals.

Table 5. Relative Spin State Energies (kcal/mol) of the Co−Co−Cl Complex Obtained with Active Spaces Containing Various Amounts of the 4*d* Shell

	(14,12)		(14,20)/(14,10)/2	
	CASSCF	CASPT2	RASSCF	RASPT2
singlet	0.0	0.0	0.0	0.0
triplet	0.8	2.0	0.9	1.6
quintet	2.4	5.6	2.8	4.5
septet	4.8	10.7	5.7	9.2

Table 6. Effect of Active Space Size on the Weights of the Dominant Configuration (DC) and Estimated EBO for the Singlet Spin State of the Co−Co−Cl Complex

	(14,12)	(14,14)	(14,20)/(14,10)/2
weight of DC	19%	17%	14%
EBO	0.22	0.22	0.25

current results suggest that only the LDA functional describes correctly the Fe−Fe−Cl complex, as addition of more than 12% exact exchange to the PBE functional, or 10% exact exchange to the TPSS functional, results in the prediction of an incorrect ground spin state, Figure 4.

In contrast to the situation obtained for Fe−Fe−Cl, the hybrid B3LYP, PBE0-(12%, 25%, and 50%) functionals as well as the metahybrid TPSSh, M06, and M06-2X functionals correctly predict the ground spin states of Co−Co−Cl, Co−Mn−Cl, Co−Fe−Cl, and Fe−Mn−Cl (see the Supporting Information). The Fe−Fe−Cl species likely features a greater amount of delocalization or bonding across its intermetallic distance than Co−Co−Cl, Co−Mn−Cl, Co−Fe−Cl, and Fe−Mn−Cl, consistent with its significantly shorter M_1-M_2 distance (2.29 Å in Fe−Fe−Cl in contrast to 2.49−2.53 Å for the other complexes). It would then be reasonable to suspect that the greater localization of molecular orbitals that is likely associated with the presence of exact exchange is the culprit for the stabilization of the nonet and singlet states of Fe−Fe−Cl, Figure 4.

In Figure 5, we show the spin density distribution plots of the broken-symmetry singlet and septet states of Fe−Fe−Cl obtained with the PBE functional. We also present the spin density difference plots obtained with the PBE0-(12%, 25%, and 50%) functionals while using the spin density plot obtained with PBE as a reference. For the septet state, addition of increasing amounts of exact exchange results in excess α-electron spin density at Fe_2 (top metal) and a reduction in the α-electron spin density at Fe_1 (bottom metal). On the other hand, for the singlet state, addition of exact exchange results in greater spin polarization: greater β-electron spin density at Fe_1 (bottom metal) and greater α-electron spin density at Fe_2 (top metal), Figure 5. These plots confirm that electron

DOI: 10.1021/acs.jctc.5b00412
J. Chem. Theory Comput. 2015, 11, 4093−4101

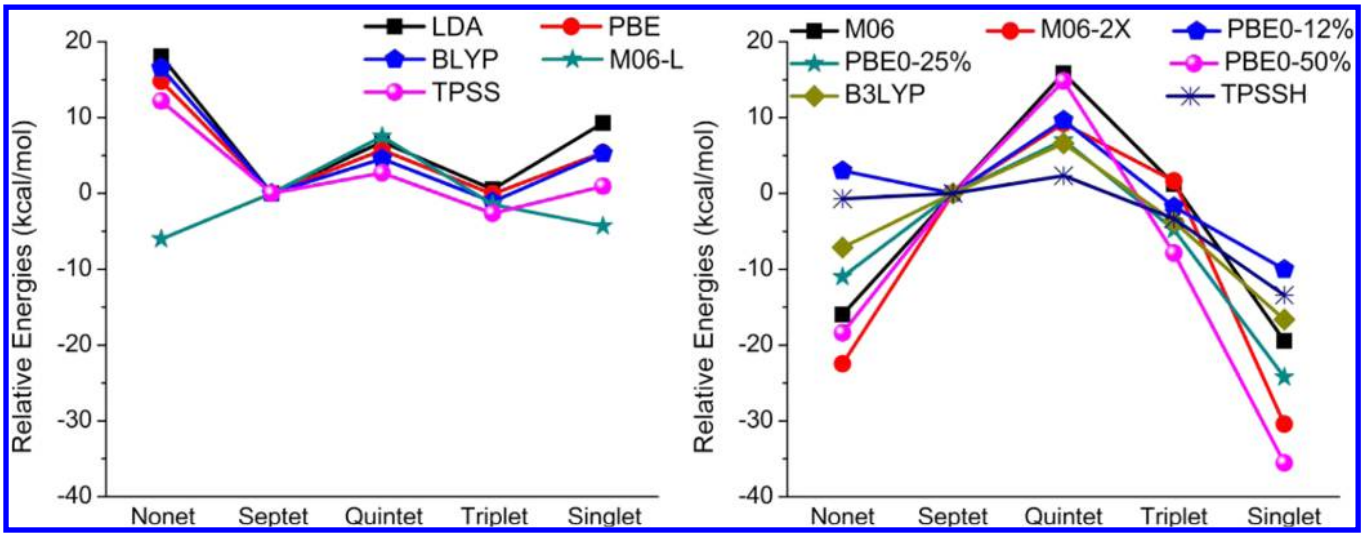

Figure 4. Calculated relative energies of various electronic spin states of Fe−Fe−Cl obtained with several (left) local and (right) hybrid exchange-correlation functionals. The energies of the various states are given relative to the energy of the septet state.

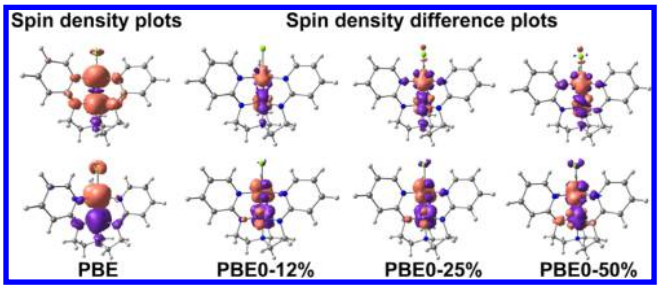

Figure 5. Spin density distribution plots of the septet (top) and broken-symmetry singlet (bottom) states of Fe−Fe−Cl obtained with the PBE functional. The spin density difference plots of Fe−Fe−Cl obtained with PBE0−12%, PBE0−25%, and PBE0−50% are obtained with respect to PBE as a reference.

delocalization across the Fe−Fe distance will be lower when hybrid functionals are used. We note that the propensity of various exchange-correlation functionals to yield different spin density distributions for low-spin states with significant multireference character has been previously reported.[60−62]

To be more specific about the origins of the incorrect prediction of the ground state of Fe−Fe−Cl by hybrid functionals (as the spin density distribution paints a general/gross picture and increasing localization of spin density is also seen in Co−Co−Cl, Table S10), it appears that introduction of exact exchange leads to localization of the 3d orbitals involved in the bonding between the metal centers. To illustrate, in Figure 6, we show that that the π orbitals in Fe−Fe−Cl are significantly delocalized with the PBE functional. With this local functional, the two π orbitals each have about 50% contribution from Fe_1 (bottom metal) and 37% from Fe_2 (top metal). However, when the PBE0 functional is used, the π orbitals become largely localized on the bottom metal (51−71%), with very little contribution from the top metal (only 5−8%). The increase in the localization of the π orbitals by the hybrid functional is a situation that seems to be associated with incorrect ground states and spin state energetics, Figure 4. The fact that the hybrid functionals increase the localization of the π orbitals for the Fe−Fe−Cl complex and that hybrid functionals do not predict the correct relative energetics of the various spin states mimics the effect of not including the correlating 4d orbitals in the active space of the CASSCF and RASSCF calculations, Figure 3.

The Co−Co−Cl, Co−Mn−Cl, Co−Fe−Cl, and Fe−Mn−Cl species present little interaction between the two metal centers, consistent with larger intermetallic distances. The localization of orbitals and spin density distributions occurs with hybrid functionals for Co−Co−Cl, Co−Mn−Cl, Co−Fe−Cl, and Fe−Mn−Cl as well. However, in these cases, it does not have as severe of an effect as in the Fe−Fe case because the MOs of the other M−M−Cl complexes are inherently more localized, so either GGA or hybrid functionals can correctly predict relative spin state energetics.

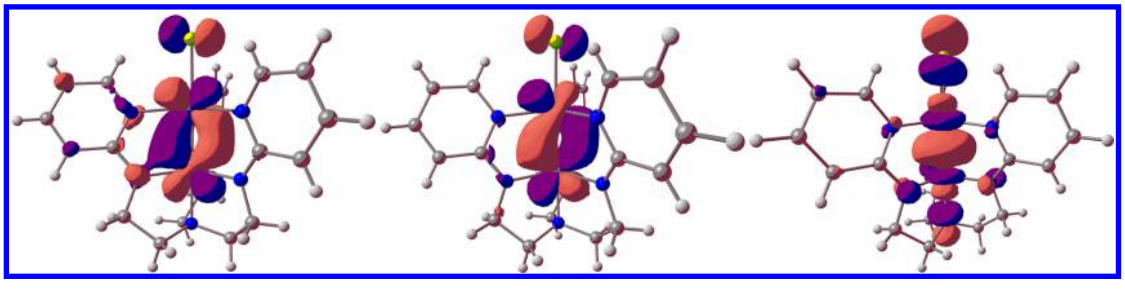

Figure 6. Series of π (left and middle) and σ (right) orbitals between the metals of Fe−Fe−Cl obtained at the PBE level of theory. The contributions to the π orbitals are 51%-Fe_1+37%-Fe_2 (left) and 49%-Fe_1+37%-Fe_2 (middle) with PBE. These orbitals become localized largely on the bottom metal when hybrid functionals are used. For example with PBE0, the contributions to the π orbitals are 56%-Fe_1+5%-Fe_2 and 71%-Fe_1+8%-Fe_2.

DOI: 10.1021/acs.jctc.5b00412
J. Chem. Theory Comput. 2015, 11, 4093−4101

Structural Properties. The structures of Co−Co−Cl, Co−Mn−Cl, Co−Fe−Cl, Fe−Fe−Cl, and Fe−Mn−Cl were optimized with several density functionals. The mean absolute errors (MAEs) are presented in Table 7. Two observations can be made. First, of the tested functionals, PBE appears to perform reasonably well, suggesting that it is a good compromise between accuracy and computational expediency.

Table 7. Mean Absolute Errors (MAE) of the Structural Properties (M−M, M−Cl, M−N Bond Distances (Å) and N−M−N Bond Angles (degrees)) Obtained at the DFT Level Compared to Experimental Structures

	LDA	BLYP	PBE	M06-L	PBE0-12	PBE0	PBE0-50
M−M	0.18	0.07	0.05	0.06	0.04	0.09	0.14
M−Cl	0.04	0.05	0.01	0.01	0.02	0.02	0.03
M−N	0.07	0.03	0.02	0.01	0.01	0.02	0.02
N−M−N	4.37	2.57	2.04	3.05	3.75	5.17	4.28

Second, the deviation between the calculated and experimental intermetallic M_1-M_2 distance is largest for LDA and hybrid density functionals containing in excess of 20% exact exchange. This situation is observed for the highly delocalized Fe−Fe−Cl complex as well as the cobalt complexes, possessing greater amounts of localization of the metal 3*d* orbitals.

CONCLUSIONS

In this work, we have employed multiconfigurational wave functions followed by second order perturbation theory, CASPT2 and RASPT2, to correctly determine the ground spin state of a diiron (Fe−Fe−Cl) complex that features significant delocalization of the 3*d* orbitals, consistent with a very short intermetallic distance. We compared the performance of CASPT2 and RASPT2 for Fe−Fe−Cl to their performance for the analogous Co−Co−Cl, Co−Fe−Cl, Co−Mn−Cl, and Fe−Mn−Cl, systems that feature longer intermetallic distances and greater degrees of localization of the metal 3d orbitals. Lastly, we examined the performance of different types of exchange-correlation functionals for predicting the correct spin state, and the structural properties of these bimetallic complexes.

Overall for Fe−Fe−Cl, an active space that includes the full 4*d* shell is necessary to accurately describe the bonding and relative spin state energetics. In contrast, for the analogous Co−Co−Cl, a complex with localized metal centers, we obtain essentially the same result with either inclusion of full 4*d* shell or a truncated 4*d* shell in the active space. On the other hand, for Fe−Fe−Cl, only when the π/π^* pair is added to the active space will the correct electronic structure and ground state be predicted.

The need to capture bonding via delocalization of 3*d* atomic orbitals as π and σ molecular orbitals between the iron centers of Fe−Fe−Cl also extend to density functional theory methods. Pure exchange correlation functionals are able to correctly predict the ground spin state of Fe−Fe−Cl as well as those of the other members of the M_1-M_2-Cl series. Inclusion of exact exchange however results in greater localization of the 3*d* atomic orbitals, resulting in a failure to properly describe the intermetallic bonding in Fe−Fe−Cl, a situation that is associated with incorrect prediction of the ground spin states as well as poorer agreement of calculated structural properties with available experimental data.

ASSOCIATED CONTENT

Supporting Information

The Supporting Information is available free of charge on the ACS Publications website at DOI: 10.1021/acs.jctc.5b00412.

Details on the various CASSCF and RASSCF calculations attempted for each spin state, orbital diagrams for the correlation orbitals of the septet state of Fe−Fe−Cl for (12,15) and (12,20)/(12,10)/2 active spaces, DFT energies for various spin states of Co−Mn−Cl, Co−Fe−Cl, Co−Co−Cl, and Fe−Mn−Cl, and tabulated spin densities for (12,15) and (12,20)/(12,10)/2 active spaces for the septet spin state of Fe−Fe−Cl (PDF)

AUTHOR INFORMATION

Corresponding Author

*E-mail: gagliardi@umn.edu.

Notes

The authors declare no competing financial interest.

ACKNOWLEDGMENTS

This work was supported as part of the Inorganometallic Catalyst Design Center, an Energy Frontier Research Center funded by the U.S. Department of Energy (DOE), Office of Science, Basic Energy Sciences (BES), under Award DE-SC0012702.

REFERENCES

(1) Löwdin, P. O. *Phys. Rev.* **1955**, *97*, 1509−1520.
(2) Mok, D. K. W.; Neumann, R.; Handy, N. C. *J. Phys. Chem.* **1996**, *100*, 6225−6230.
(3) Hollett, J. W.; Gill, P. M. W. *J. Chem. Phys.* **2011**, *134*, 114111.
(4) Handy, N. C.; Cohen, A. J. *Mol. Phys.* **2001**, *99*, 403−412.
(5) Kohn, W.; Sham, L. J. *Phys. Rev.* **1965**, *140*, A1133−A1138.
(6) Cohen, A. J.; Mori-Sánchez, P.; Yang, W. *Science* **2008**, *321*, 792−794.
(7) Harvey, J. N. On the accuracy of density functional theory in transition metal chemistry. *Annu. Rep. Prog. Chem., Sect. C: Phys. Chem.* **2006**, *102*, 203−226.
(8) Schultz, N. E.; Zhao, Y.; Truhlar, D. G. *J. Phys. Chem. A* **2005**, *109*, 11127−11143.
(9) Rong, C.; Lian, S.; Yin, D.; Shen, B.; Zhong, A.; Bartolotti, L.; Liu, S. *J. Chem. Phys.* **2006**, *125*, 174102.
(10) Rong, C.; Lian, S.; Yin, D.; Zhong, A.; Zhang, R.; Liu, S. *Chem. Phys. Lett.* **2007**, *434*, 149−154.
(11) Sorkin, A.; Iron, M. A.; Truhlar, D. G. *J. Chem. Theory Comput.* **2008**, *4*, 307−315.
(12) Swart, M. *J. Chem. Theory Comput.* **2008**, *4*, 2057−2066.
(13) Reiher, M.; Salomon, O.; Hess, B. A. *Theor. Chem. Acc.* **2001**, *107*, 48−55.
(14) Lovell, T.; Han, W. G.; Liu, T.; Noodleman, L. *J. Am. Chem. Soc.* **2002**, *124*, 5890−5894.
(15) Noodleman, L.; Norman, J. G.; Osborne, J. H.; Aizman, A.; Case, D. A. *J. Am. Chem. Soc.* **1985**, *107*, 3418−3426.
(16) Roos, B. O.; Taylor, P. R.; Siegbahn, P. E. M. *Chem. Phys.* **1980**, *48*, 157−173.
(17) Andersson, K.; Malmqvist, P. A.; Roos, B. O.; Sadlej, A. J.; Wolinski, K. *J. Phys. Chem.* **1990**, *94*, 5483−5488.
(18) Siegbahn, P. E. M.; Almlof, J.; Heiberg, A.; Roos, B. O. *J. Chem. Phys.* **1981**, *74*, 2384−2396.
(19) Isley, W. C., III; Zarra, S.; Carlson, R. K.; Bilbeisi, R. a; Ronson, T. K.; Nitschke, J. R.; Gagliardi, L.; Cramer, C. J. *Phys. Chem. Chem. Phys.* **2014**, *16*, 10620−10628.
(20) Vancoillie, S.; Zhao, H.; Radoń, M.; Pierloot, K. *J. Chem. Theory Comput.* **2010**, *6*, 576−582.

DOI: 10.1021/acs.jctc.5b00412
J. Chem. Theory Comput. 2015, 11, 4093−4101

(21) Olsen, J.; Roos, B. O.; Jørgensen, P.; Jensen, H. J. A. *J. Chem. Phys.* **1988**, *89*, 2185.
(22) Ma, D.; Li Manni, G.; Gagliardi, L. *J. Chem. Phys.* **2011**, *135*, 044128.
(23) Li Manni, G.; Ma, D.; Aquilante, F.; Olsen, J.; Gagliardi, L. *J. Chem. Theory Comput.* **2013**, *9*, 3375−3384.
(24) Ivanic, J. *J. Chem. Phys.* **2003**, *119*, 9377−9385.
(25) Ivanic, J.; Ruedenberg, K. Identification of deadwood in configuration spaces through general direct configuration interaction. *Theor. Chem. Acc.* **2001**, *106*, 339−351.
(26) Chan, G. K.-L.; Sharma, S. *Annu. Rev. Phys. Chem.* **2011**, *62*, 465−481.
(27) Marti, K. H.; Ondík, I. M.; Moritz, G.; Reiher, M. *J. Chem. Phys.* **2008**, *128*, 014104.
(28) Neuscamman, E.; Yanai, T.; Chan, G. K. L. *J. Chem. Phys.* **2009**, *130*, 124102.
(29) Yanai, T.; Kurashige, Y.; Ghosh, D.; Chan, G. K. L. *Int. J. Quantum Chem.* **2009**, *109*, 2178−2190.
(30) Ghosh, D.; Hachmann, J.; Yanai, T.; Chan, G. K. L. *J. Chem. Phys.* **2008**, *128*, 144117.
(31) Li Manni, G.; Carlson, R. K.; Luo, S.; Ma, D.; Olsen, J.; Truhlar, D. G.; Gagliardi, L. *J. Chem. Theory Comput.* **2014**, *10*, 3669−3680.
(32) Ghosh, A. *JBIC, J. Biol. Inorg. Chem.* **2006**, *11*, 712−724.
(33) Neese, F.; Zaleski, J. M.; Loeb Zaleski, K. L.; Solomon, E. I. *J. Am. Chem. Soc.* **2000**, *122*, 11703−11724.
(34) Tereniak, S. J.; Carlson, R. K.; Clouston, L. J.; Young, V. G., Jr.; Bill, E.; Maurice, R.; Chen, Y.; Kim, H. J.; Gagliardi, L.; Lu, C. C. *J. Am. Chem. Soc.* **2014**, *136*, 1842−1855.
(35) Clouston, L. J.; Siedschlag, R. B.; Rudd, P. A.; Planas, N.; Hu, S.; Miller, A. D.; Gagliardi, L.; Lu, C. C. *J. Am. Chem. Soc.* **2013**, *135*, 13142−13148.
(36) Malmqvist, P. A.; Pierloot, K.; Shahi, A. R. M.; Cramer, C. J.; Gagliardi, L. *J. Chem. Phys.* **2008**, *128*, 204109.
(37) Aquilante, F.; De Vico, L.; Ferré, N.; Ghigo, G.; Malmqvist, P.-Å; Neogrády, P.; Pedersen, T. B.; Pitonak, M.; Reiher, M.; Roos, B. O.; Serrano-Andrés, L.; Urban, M.; Veryazov, V.; Lindh, R. *J. Comput. Chem.* **2010**, *31*, 224−247.
(38) Reiher, M. *Wiley Interdiscip. Rev. Comput. Mol. Sci.* **2012**, *2*, 139−149.
(39) Roos, B. O.; Lindh, R.; Malmqvist, P.-Å.; Veryazov, V.; Widmark, P.-O. *J. Phys. Chem. A* **2005**, *109*, 6575.
(40) Roos, B. O.; Veryazov, V.; Widmark, P.-O. *Theor. Chem. Acc.* **2004**, *111*, 345.
(41) Aquilante, F.; Lindh, R.; Pedersen, T. B. *J. Chem. Phys.* **2007**, *127*, 114107.
(42) Forsberg, N.; Malmqvist, P.-Å. *Chem. Phys. Lett.* **1997**, *274*, 196−204.
(43) Roos, B. O.; Borin, A. C.; Gagliardi, L. *Angew. Chem., Int. Ed.* **2007**, *46*, 1469−1472.
(44) Te Velde, G.; Bickelhaupt, F. M.; van Gisbergen, S. J.; Fonseca Guerra, C.; Baerends, E. J.; Snijders, J. G.; Ziegler, T. *J. Comput. Chem.* **2001**, *22*, 931.
(45) Van Lenthe, E. *J. Comput. Chem.* **1999**, *20*, 51.
(46) Van Lenthe, E.; Baerends, E. J.; Snijders, J. G. *J. Chem. Phys.* **1993**, *99*, 4597.
(47) Vosko, S. H.; Wilk, L.; Nusair, M. *Can. J. Phys.* **1980**, *58*, 1200−1211.
(48) Becke, A. D. *Phys. Rev. A: At., Mol., Opt. Phys.* **1988**, *38*, 3098−3100.
(49) Lee, C.; Yang, W.; Parr, R. G. *Phys. Rev. B: Condens. Matter Mater. Phys.* **1988**, *37*, 785−789.
(50) Adamo, C.; Barone, V. *J. Chem. Phys.* **1999**, *110*, 6158.
(51) Perdew, J. P.; Burke, K.; Ernzerhof, M. *Phys. Rev. Lett.* **1996**, *77*, 3865−3868.
(52) Tao, J. M.; Perdew, J. P.; Staroverov, V. N.; Scuseria, G. E. *Phys. Rev. Lett.* **2003**, *91*, 146401.
(53) Zhao, Y.; Truhlar, D. G. *J. Chem. Phys.* **2006**, *125*, 194101.
(54) Zhao, Y.; Truhlar, D. G. *Theor. Chem. Acc.* **2008**, *120*, 215−241.
(55) Becke, A. D. *J. Chem. Phys.* **1993**, *98*, 5648−5652.
(56) Stephens, P. J.; Devlin, F. J.; Chabalowski, C. F.; Frisch, M. J. *J. Phys. Chem.* **1994**, *98*, 11623−11627.
(57) Zall, C. M.; Zherebetskyy, D.; Dzubak, A. L.; Bill, E.; Gagliardi, L.; Lu, C. C. *Inorg. Chem.* **2012**, *51*, 728−736.
(58) Kim, J.; Kim, J. *Chem. Phys. Lett.* **2014**, *592*, 24−29.
(59) Lawson Daku, L. M.; Vargas, A.; Hauser, A.; Fouqueau, A.; Casida, M. E. *ChemPhysChem* **2005**, *6*, 1393−1410.
(60) Boguslawski, K.; Jacob, C. R.; Reiher, M. *J. Chem. Theory Comput.* **2011**, *7*, 2740−2752.
(61) Boguslawski, K.; Marti, K. H.; Legeza, Ö.; Reiher, M. *J. Chem. Theory Comput.* **2012**, *8*, 1970−1982.
(62) Conradie, J.; Ghosh, A. *J. Phys. Chem. B* **2007**, *111*, 12621−12624.

DOI: 10.1021/acs.jctc.5b00412
J. Chem. Theory Comput. 2015, 11, 4093−4101